Sādhanā (2020) 45:281
https://doi.org/10.1007/s12046-020-01507-x

A unified method to the design of an improved high frequency sliding mode current controller for DC/DC boost converter in continuous current condition based on analogue implementation

ALIREZA GOUDARZIAN* and ADEL KHOSRAVI

Department of Electrical Engineering, Faculty of Engineering, Shahrekord Branch, Islamic Azad University, Shahrekord, Iran
e-mail: a.goudarzian@eng.ui.ac.ir; alireza9071@gmail.com

MS received 10 May 2018; revised 5 March 2020; accepted 23 September 2020

Abstract. In this study, an improved high frequency sliding mode current controller is proposed for DC/DC power converters in continuous current condition using analogue-based implementation. The sliding mode control is a variable frequency method. In this strategy, the controller frequency is a function of summation of all time delays of different parts of control circuit. If these delays increase, the switching frequency extremely decreases, steady error of the output voltage increases; and also, the converter frequency may be less than the audible frequency. In practical applications, it is extremely important that the output voltage tracks exactly its reference signal. Moreover, the switching frequency of a power converter must be more than 20 kHz in practice. A good way for enhancement of the switching frequency and dynamical performance of the sliding mode method is to use all state variables of the controlled system in the sliding manifold. This attempt has been made for the voltage regulation and input current control of a typical Boost converter in this paper. Using sliding mode theory and Filippov's method, the stability of the suggested controller is established. Simulations and practical implementation of the proposed system show that the developed controller is successful to control the converter at high frequencies by removing the voltage error in steady region, despite using low speed and cheap electrical devices in the control circuit.

Keywords. Sliding mode control; power converters; dynamical performance; switching frequency; analogue implementation.

1. Introduction

Nowadays, DC/DC energy conversion systems have been commonly used for solar panels, computer equipment, power sources and industrial applications [1–5]. These converters are placed in three types; namely, buck, boost and buck-boost. The Boost converter can be used to step-up the input voltage. This converter has the advantages of high power density, high efficiency and simple structure. Hence, the Boost converter has been selected for this paper. The circuit topology of a Boost converter is depicted in figure 1a.

From control point of view, the nature of the Boost converter is non-minimum phase. This leads to complicated dynamic behavior and slow response. The non-minimum phase systems inherit the right half plane zero characteristics. Hence, a Boost converter suffers from very small phase margin [6]. The mentioned problem makes the converter more sensitive to time delays. The first objective for the performance enhancement of a Boost converter is to fix the converter voltage at a desired value. A common method for stabilizing power switching converters is application of classical controllers such as proportional-integral (PI) and proportional-integral-derivative (PID) controllers [7–9]. The construction of PI and PID is simple and feasible. However, these methods are sensitive to load and voltage variations, because they are designed based on the linearized small signal model of DC/DC converters. On the other hand, the Boost converter is a non-linear system. Hence, non-linear controllers are more suitable for DC/DC converters.

In [10], the input-output feedback linearization method is applied to control the velocity of a synchronous motor supplied by a Boost converter. However, the presented controller needs to the exact model of the developed system. In the references [11, 12], indirect adaptive back-stepping method is used for DC/DC converters. But, by using this controller, an inherent steady state error will be existed in the output voltage.

In [13–16], peak current mode strategy has been applied to improve dynamical behavior of DC/DC power

*For correspondence
Published online: 10 November 2020

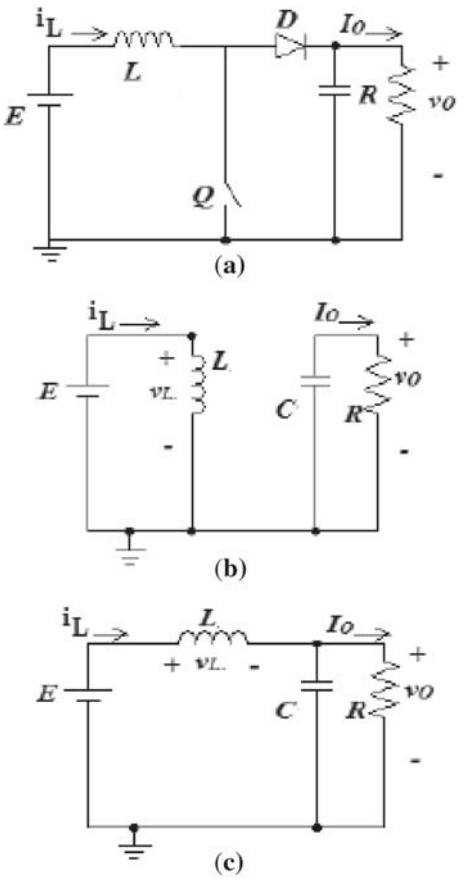

Figure 1. The CCM operation of a typical Boost converter; (a) the converter diagram; (b) the converter during switch-ON state; (c) the converter during switch-OFF state.

converters. The proposed control approach is famous for its inherent protection against overload and input current regulation. However, it has a major problem of requirement to an external triangular signal for compensation. Hence, the application of peak current mode controller leads to other problems such as ringing noise, large time delays, voltage ripple increment, slow dynamical response, etc. Also, this controller is developed using small signal analysis. It is not able to ensure robustness and stability of DC/DC converters in various operating conditions.

In the past years, sliding mode control (SMC) has been broadly utilized for variable structure systems [17]. SMC has many merits compared with other non-linear controllers such as good dynamical response, high robustness against uncertainties and relative ease of construction. There are two main techniques to develop a SMC for better stability of a highly non-linear converter; namely, indirect and direct methods. In the first method, after selecting a suitable sliding manifold S, equivalent control law is given by solving $\dot{S} = 0$. Also, there exists two general methods to generate switching signal for driving the switch of DC/DC converters. The first switching technique uses a carrier waveform with a variable amplitude [18, 19]. In the second switching method, a ramp signal with s constant magnitude and fixed frequency is applied for pulse width modulation [20–22]. A constant frequency PWM SMC is not designed using the Lyapunov function. Thus, this controller is not robust against the output voltage variations and parameter uncertainties. Also, there exists a small steady error in the output voltage as compared to its reference signal. Hence, the direct SMC is more popular. In addition, the switching operation of a DC/DC converter under the direct method is performed using parabolic or hysteresis modulation methods [23–25]. The direct method ensures the excellent behavior of the load voltage of DC/DC converters as compared with the indirect type. The frequency of a converter with direct SMC is dependent to sampling frequency and time delays of electronic devices used in command and control circuits. If low speed components are used for construction of the controller, the switching frequency extremely decreases. The low frequency increases electromagnetic interferes, vibration, losses, current and voltage ripples, etc. Also, a DC/DC converter with the traditional SMC may be entered to discontinuous current condition. However, it is better for a power converter to remain in continuous conduction mode. Only way for switching frequency increment is application of high speed and expensive devices which can increase the costs.

In addition to aforementioned works, a simple SMC based on digital implementation is proposed for DC/DC converters in [26–28]. However, the digital control has a major problem, which reduces sampling frequency. Thus, the system switching frequency with the traditional SMC is low. By observing the practical tests in [26, 27], it is seen that the system frequency is nearly 10 kHz for all the experiments, provided in this study. However, the system frequency should be higher compared with the audible frequency. It is better for switching converters to operate in interval of [20 300] kHz [29]. It is impossible to keep the frequency of a typical SMC at very high switching frequencies with fast response, robust performance, low cost and high sampling frequency by using digital implementation.

This paper proposes a PD-PI type SMC applied to a Boost converter. The proposed controller is able to regulate the converter voltage with zero steady error via a PI controller and stabilize the non-minimum phase converter using a PD controller. The system stability analysis is not straightforward. Hence, the sliding mode control concepts and Filippov's technique are used to investigate the controller behavior. In this paper, it will be proved that utilization of the PD in the sliding manifold successfully enhances the frequency of the converter, because time derivative of the proposed sliding manifold or equivalently, speed of the sliding manifold will be a function of the impulse function. Therefore, the sliding regime can be achieved with a very high frequency. Also, it will be proved that the Boost converter dynamics cannot be stabilized

without using the input current. To reach a fast response, satisfactory performance and high sampling frequency, the analog implementation is used in this paper. Furthermore, it will be shown via simulation results that the proposed approach in [26–28] cannot be used when the converter works in light load conditions.

Based on the aforementioned discussions, the presented paper is organized as follows: in section 2, the design of the suggested SMC is performed for a Boost converter and the stability analysis of the controlled system is investigated in section 3. Simulations are given in section 4. In section 5, the practical experiments are shown. The more discussions are introduced in section 6 and finally, conclusions are provided in section 7.

2. The proposed system

2.1 *The converter model in continuous current mode*

The typical topology of a Boost converter is shown in figure 1a. In this figure, Q, D, E, R, L, C denote the switch, diode, input voltage, load, inductor and capacitor. Also, v_O is the output voltage and i_L is the inductor current. In this section, the converter parameters are considered to be ideal. Figure 1b illustrates that the Boost converter when the switch conducts. Furthermore, figure 1c shows the converter in switch-OFF state. The mathematical equation of the converters is determined as follows:

$$\begin{cases} \dfrac{di_L}{dt} = \dfrac{E}{L} - \dfrac{(1-u)(v_O)}{L} \\ \dfrac{dv_O}{dt} = \dfrac{(1-u)i_L}{C} - \dfrac{v_O}{RC} \end{cases} \tag{1}$$

where u is the instantaneous state of the switch. u is 1 for switch-On state and 0 for switch-OFF condition. By solving $\frac{di_L}{dt} = \frac{dv_O}{dt} = 0$, the steady state point of equation (1) can be obtained as:

$$V_O = V_d, I_L = \frac{V_d^2}{RE}, U = 1 - \frac{E}{V_d} \tag{2}$$

where V_d is the voltage reference. Also, V_O, I_L and U are the mean value of the output voltage, inductor current and duty cycle of the converter, respectively. Furthermore, the following limitation exists for a Boost converter:

$$E\langle v_O, i_L\rangle 0, 0 < U < 1 \tag{3}$$

2.2 *Design of an improved high frequency sliding mode current controller (IHFSMCC)*

Due to non-minimum phase structure of the converter, it is necessary to control the converter current. Otherwise, the converter will be unstable. On the other hand, the output voltage must be regulated at a fixed value with no steady error. To this end, a PI compensator should be taken into consideration for the voltage regulation. To control the converter at high frequencies, a feed-forward control scheme is applied according to the converter current and its derivative. The suggested sliding manifold is considered as follows:

$$S = a_1 i_L + i_{Lref} \tag{4}$$

where i_{Lref} is the current reference signal and defined as follows:

$$i_{Lref} = a_2(v_O - V_d) + a_3 \int_0^t (v_O - V_d)dt + a_4 i_L' \tag{5}$$

where i_L' is the time derivative of the converter current. The mean value of i_L' will be zero in steady region. However, the instantaneous value of i_L' will be proportional to the step function (see (1)). Hence, the time derivative of i_L' will be a function of the impulse function ($u'(t) = \delta(t)$). Therefore, the impulse function appears in the time derivative of the sliding variable. It will be established that this strategy allows the SMC to work with a high frequency. According to (4) and (5), the defined sliding manifold is obtained as:

$$S = a_1 i_L + a_2(v_O - V_d) + a_3 \int_0^t (v_O - V_d)dt + \frac{a_4}{L} v_L, v_O \; / \; = 0 \tag{6}$$

Figure 2 shows the implementation way of the proposed controller. Also, the hysteresis (bang-bang) control law for control of the switch is described as:

$$u = \begin{cases} 0 = OFF & when\ S > \varepsilon_1 \\ 1 = ON & when\ S < -\varepsilon_2 \\ unchanged & otherwise \end{cases} \tag{7}$$

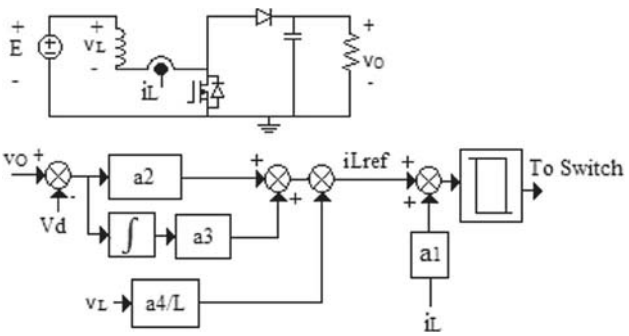

Figure 2. The general control scheme bandwidth.

where $\varepsilon_1 > 0$ and $\varepsilon_2 > 0$ are the hysteresis bandwidths. Figure 3 illustrates that how a hysteresis bandwidth is produced using the sliding manifold. The switch will conduct when S becomes less than $-\varepsilon_2$ and switch will be open when S becomes larger than ε_1. When the sliding regime is achieved, all the phase trajectories and deigned sliding manifold approach to zero, i.e., $S = 0$. Therefore, the term $\int_{t_{reach}}^{t}(v_O - V_d)dt$ converges to zero, where t_{reach} is the settling time of the controlled system. Hence, the term $v_O - V_d$ vanishes and the control objective is achieved. Also, the proposed sliding manifold is a linear surface in the phase portrait. It is obvious that a highly non-nonlinear system is transformed to a simple linear system. This is an extremely important property of SMCs. From (7), it is found that there is no gain in the hysteresis control law. The limited disturbances, controller parameters and operating regions don't impact on equation (7). Thus, the controller will be robust to parametric uncertainties, load variations and input voltage changes. It is necessary to prove the stability of the developed linear sliding manifold. To this end, the following sections discuss about the dynamical and steady state characteristics of the IHFSMCC.

3. Investigation of the stability of the IHFSMCC

To study the controller stability, the existence condition and stability condition must be investigated [30]. For achievement of these purposes, the first condition is checked using Lyapunov theory and the second one is checked based on the Filippov's technique. The conditions are discussed latter.

3.1 *Existence condition*

We choose a positive Lyapunov function candidate as follows:

$$F = \frac{1}{2}S^2 \tag{8}$$

The derivative of the sliding variable is determined as follows:

$$S' = i'_{Lref} + a_1 i'_L = i'_{Lref} + a_1 \frac{1}{L}[E - (1-u)(v_O)] \tag{9}$$

By replacing (9) into (8), it yields:

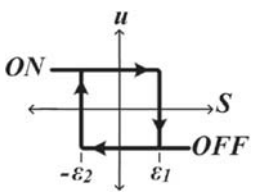

Figure 3. Figure illustrating the production of the hysteresis.

$$F' = SS' = S\left(i'_{Lref} + a_1\frac{1}{L}[E-(1-u)(v_O)]\right) \rightarrow F' = \frac{1}{L}S\left(Li'_{i_{Lref}} + a_1[E-(1-u)(v_O)]\right) \tag{10}$$

If $S > \varepsilon_1$, then $u = 0$. Thus, the equation (10) is simplified as follows:

$$F' = \frac{1}{L}S\left(Li'_{Lref} + a_1[E - v_O]\right) \tag{11}$$

If $S < -\varepsilon_2$, then $u = 1$. Thus, the equation (10) is transformed into the following equation:

$$F' = \frac{1}{L}S\left(Li'_{Lref} + a_1 E\right) \tag{12}$$

By combining (11) and (12), it is found:

$$F' = \frac{1}{L}\left[S\left(Li'_{Lref} + a_1E - \frac{1}{2}a_1v_O\right) - \frac{1}{2}|S|v_O\right] \rightarrow F' = \frac{1}{L}|S|[sign(S)\left(Li'_{Lref} + a_1E - \frac{1}{2}a_1v_O\right) - \frac{1}{2}a_1v_O \tag{13}$$

By considering the above equation, F' satisfies the following equation:

$$F' \le \frac{1}{L}|S|\left[\left|Li'_{Lref} + a_1E - \frac{1}{2}v_O\right| - \frac{1}{2}v_O\right] \tag{14}$$

According to the Lyapunov theory, to guarantee the sliding mode operation, F' must be negative. The following inequality ensures the sliding mode operation:

$$\begin{aligned}
&\frac{1}{L}|S|\left[\left|Li'_{Lref} + E - \frac{1}{2}a_1v_O\right| - \frac{1}{2}a_1v_O\right] < 0 \rightarrow \left|Li'_{Lref} + a_1E - a_1\frac{1}{2}v_O\right| \\
&-\frac{1}{2}a_1v_O < 0 \rightarrow \left|Li'_{Lref} + a_1E - \frac{1}{2}a_1v_O\right| < \frac{1}{2}a_1v_O \rightarrow \\
&-\frac{1}{2}a_1v_O < Li'_{Lref} + a_1E \\
&-\frac{1}{2}a_1v_O < \frac{1}{2}a_1v_O \rightarrow 0 < Li'_{Lref} + a_1E < a_1v_O
\end{aligned} \tag{15}$$

The final term of (15) denotes a domain of attraction for the controller. Generally L is very small. Hence, it can be assumed that $Li'_{Lref} \approx 0$. According to converter limitation expressed in (3), it can be understood from (15) that the obtained domain is a wide region. Also, it is concluded that if a_1 is considered zero, then the sliding manifold will be unstable. This conclusion shows the non-minimum phase behavior of the Boost converter. Therefore, the converter current should be used in the sliding manifold. As a consequence, the output voltage reference signal must be in a certain range. The first limitation is that V_d must be larger than E. If the voltage reference signal is too close to the input voltage value, the system stability could be easily deteriorated. It is recommended for the output voltage to be a larger value compared to the input voltage. With satisfaction of the existence condition, the sliding manifold

reaches to zero. Then, the equivalent control signal is given using the following equation:

$$u_{eq}^{'} = \frac{L}{-a_4 v_O}\left[a_1\frac{E}{L} - \frac{a_2 v_O}{RC} + a_3(v_O - V_d) + (1-u_{eq})[-\frac{a_1}{L}v_O + \frac{a_2 i_L}{C} - \frac{a_4}{LC}(1-u_{eq})i_L + \frac{a_4 v_O}{RLC}\right] \tag{16}$$

The controlled dynamics of the converter with proposed controller is determined as follow

$$\begin{cases} L\frac{di_L}{dt} = E - (1-u_{eq})(v_O) \\ C\frac{dv_o}{dt} = (1-u_{eq})i_L - \frac{v_O}{R} \end{cases} \tag{17}$$

By linearizing the equation (17) around the converter equilibrium point, the stability condition can be investigated.

3.2 *Stability condition*

The condition guarantees that the trajectories of the SMC remain around the converter equilibrium point in the state space. This paper presents a simple unified approach based on Filippov's method for the controller design and investigation of the stability condition. The design methodology can be used for other systems. At first, the matrices W, X and e are defined as follows:

$$\mathrm{W} = [\mathrm{w_1 w_2}]^{\mathrm{T}} = [\mathrm{I_L} V_{\mathrm{d}}]^{\mathrm{T}}, \mathrm{X} = [\mathrm{x_1 x_2}]^{\mathrm{T}} = [\mathrm{i_L} v_O]^{\mathrm{T}}, \mathrm{e} = [\ \mathrm{e_1 e_2}]^{\mathrm{T}} \tag{18}$$

where W contains the original state variables at the equilibrium point of the Boost converter, X contains all the state variables of the converter and e is the error matrix. The error variables e_1 and e_2 can be defined as:

$$\begin{cases} e_1 = x_1 - w_1 \\ e_2 = x_2 - w_2 \end{cases} \tag{19}$$

The state-space average model of the Boost converter is expressed as:

Table 1. Characteristics of the Boost converter for simulations

Symbol	Name	Value
E	Input voltage	9 V
V_O	Output voltage	30 V
L	Inductor	330 µH
C	Capacitors	100 µF
f_s	Switching frequency	300 kHz
R	Output resistance	48 Ω
I_L	Average input current	2.08 A
U	Duty cycle	0.7

$$\dot{X} = AX + Bu_{eq} + C \tag{20}$$

where u_{eq} is the equivalent control law which can be obtained by solving $S = \dot{S} = 0$. Also, the matrices A, B and C can be obtained by using the converter parameters shown in table 1 as follows:

$$A = \begin{bmatrix} 0 & -\frac{1}{L} \\ \frac{1}{C} & -\frac{1}{RC} \end{bmatrix} = \begin{bmatrix} 0 & -3030.3 \\ 10000 & -200 \end{bmatrix}, B = \begin{bmatrix} \frac{V_d}{L} \\ -\frac{I_L}{C} \end{bmatrix} = \begin{bmatrix} 90909.09 \\ -20000 \end{bmatrix}, C = \begin{bmatrix} \frac{E}{L} \\ 0 \end{bmatrix} = \begin{bmatrix} 27272.72 \\ 0 \end{bmatrix} \tag{21}$$

The sliding manifold of the Boost converter can be expressed as (22):

$$\begin{aligned} S &= a_1 i_L + a_2(v_O - V_d) + a_3\int_0^t (v_O - V_d)dt + a_4 v_L \\ &= a_1(x_1 - w_1) + a_1 w_1 + a_2(x_2 - w_2) + a_3\int_0^t (x_2 - w_2)dt \\ &\quad + a_4\left(i_L^{'} - w_1^{'}\right) \\ &= N_1 e + N_2\int_0^t e dt + N_3 e' + N_4 W \end{aligned} \tag{22}$$

where

$$N_1 = [a_1 a_2], N_2 = [0 a_3], N_3 = [a_4 0], N_4 = [a_1 0] \tag{23}$$

The control objective is to remain all the state variables on the desired sliding manifold and enforce all the error variables to vanish. The dynamic behavior of the Boost converter can be determined by tuning the coefficients of the IHFSMCC. The state-space matrix of the converter can be rewritten as follows:

$$X = e + W \tag{24}$$

Then, the time derivative of X is given as:

$$X' = e' + W' \overset{W'=0}{\rightarrow} X' = e' \tag{25}$$

Using (20), (24) and (25), e' and e'' are expressed as follows:

$$e' = Ae + AW + Bu_{eq} + C \tag{26-a}$$

$$e'' = Ae' + AW' + Bu_{eq}^{'} + C' \overset{W'=C'=0}{\rightarrow} e'' = Ae' + Bu_{eq}^{'} \tag{26-b}$$

Consider the sliding manifold given in (22). Substituting (26-a) in (22), it yields:

$$S = N_1 e + N_2 \int_0^t e dt + N_3 A e + N_3 A W + N_3 B u_{eq} + N_3 C + N_4 W \tag{27}$$

Consider the Filippov's law. Solving $S = 0$, the equivalent control law of the proposed system can be obtained as follows:

$$u_{eq} = -[N_3 B]^{-1} \left[N_1 e + N_2 \int_0^t e dt + N_3 A e + N_3 A W + N_3 C + N_4 W \right] \tag{28}$$

Differentiating (28) with respect to time, it is given:

$$u'_{eq} = -[N_3 B]^{-1} [N_1 e' + N_2 e + N_3 A e'] \tag{29}$$

By replacing (29) in (26-b), the dynamical equation of the error system can be given by:

$$e'' + \left(-A + B[N_3 B]^{-1} [N_1 + N_3 A] \right) e' + B[N_3 B]^{-1} N_2 e = 0 \tag{30}$$

The equation (30) will be stable if the following inequalities are satisfied:

$$\left| \left(A + B[n_3 B]^{-1} [n_1 + n_3 A] \right) \right| \geq 0, |B[n_3 B]^{-1} n_2| \geq 0 \tag{31}$$

Where $|f|$ returns the determinant of f. By using (31), the values of the controller coefficients are found as:

$$0 \langle a_2 \langle a_1, a_3 \rangle 0, a_4 \rangle 0 \tag{32}$$

Consider (30). We rewritten the equation (30) as follows:

$$e'' + Ke' + Le = 0 \tag{33}$$

where

$$K = \begin{bmatrix} k_{11} & k_{12} \\ k_{21} & k_{22} \end{bmatrix}, L = \begin{bmatrix} l_{11} & l_{12} \\ l_{21} & l_{22} \end{bmatrix} \tag{34}$$

and also

$$\begin{aligned} k_{11} &= \frac{a_1}{a_4}, k_{12} = \frac{a_2}{a_4}, k_{21} = -\frac{LGa_1}{CRa_4} - \frac{1}{C}, k_{22} \\ &= -\frac{LG\left(a_2 - \frac{a_4}{L}\right)}{CRa_4} + \frac{1}{RC}, l_{11} = l_{21} = 0, l_{12} = \frac{a_3}{a_4}, l_{22} \\ &= -\frac{a_3}{a_4}\frac{LG}{CR} \end{aligned} \tag{35}$$

where $G = v_O/E$ is the voltage gain of the converter.

The state space equation corresponding to the error voltage e_2 can be derived as follows:

$$e_2''' + h_1 e_2'' + h_2 e_2' + h_3 e_2 = 0 \tag{36}$$

where:

$$\begin{aligned} h_1 &= k_{22} + k_{11}, h_2 = l_{22} + k_{11} k_{22} - k_{12} k_{21}, h_3 \\ &= k_{11} l_{22} - k_{21} l_{12} \end{aligned} \tag{37}$$

Consider $p_i (i = 1, 2, 3)$ to be the desired poles of the controlled system corresponding to the output voltage error. The system poles are obtained by:

$$\sigma^3 + h_1 \sigma^2 + h_2 \sigma + h_3 = (\sigma + p_1)(\sigma + p_2)(\sigma + p_3) \tag{38}$$

We select the parameters of the IHFSMCC as: $a_1 = 1, a_2 = 0.2, a_3 = 40, a_4 = 0.2L$. Corresponding to these values, the closed loop system poles are obtained as: $p_1 = -958.7012$, $p_{2,3} = -6.1494 \mp 45.2584i$ for the nominal operating point of the Boost converter which is described in table 1. Figure 4 shows the system poles corresponding to the output voltage for different voltage gains. From figure 4, it is realized that the real part of the dominant poles of the controlled system approaches to zero, when the voltage gain increases. Also, the imaginary part of the dominant poles decreases against increment of the voltage gain. As a result, the voltage response will be slow in high voltage gains and oscillatory in low voltage gains. Hence, the error dynamics around the origin $(0, 0)$ is at least semi-globally stable with a large domain of attraction. The sliding manifold is obtained in the stability region as follows:

$$S = \begin{cases} (N_3 A + N_1) X - (N_1 - N_4) W + N_3 C \, for \, S > \varepsilon_1 \\ (N_3 A + N_1) X + N_3 B - (N_1 - N_4) W + N_3 C \, for \, S < -\varepsilon_2 \end{cases} \tag{39}$$

Equation (39) can be expressed as (40).

$$S = \begin{cases} \sigma_1(X) = x_1 - 605.86 x_2 + 5446.9 \, for \, S > \varepsilon_1 \\ \sigma_2(X) = x_1 - 605.86 x_2 + 23629 \, for \, S < -\varepsilon_2 \end{cases} \tag{40}$$

Equations $\sigma_1 = 0$ and $\sigma_2 = 0$ defines two lines in the phase plane. These lines oscillate around the origin. The equation σ_1 represents the sliding manifold for switch-OFF condition and the equation σ_2 represents the sliding manifold for switch-ON condition. The trajectories of the Boost converter in the state space using IHFSMCC for the designed coefficients are shown in figure 5.

3.3 *The calculation of the switching frequency*

Boost converter under the IHMSMCC can operate at very high switching frequencies compared with conventional SMC. The switching performance of the Boost converter under the suggested controller is shown in figure 5. The system frequency can be derived using the following equation:

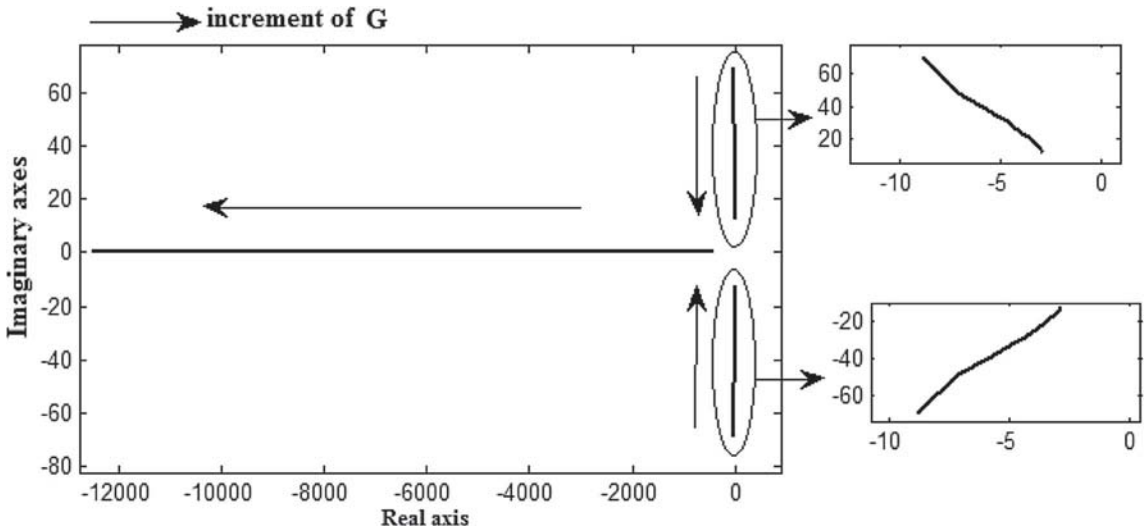

Figure 4. Root locus criterion for the developed system, $R = 48\ \Omega$, $L = 0.00033\,\text{H}$, $C = 0.0001\,\text{F}$, $G > 1$.

$$f_s = \frac{1}{\Delta t_1 + \Delta t_2} \tag{41}$$

where Δt_1 and Δt_2 are the time duration of the switch-ON and switch-OFF states, respectively. The defined parameters are given as:

$$\Delta t_1 = \frac{\Delta S}{S'|_{u=1}} = \frac{\varepsilon_1 + \varepsilon_2}{S'|_{u=1}} \tag{42 - a}$$

$$\Delta t_2 = \frac{\Delta S}{-S'|_{u=0}} = \frac{\varepsilon_1 + \varepsilon_2}{-S'|_{u=0}} \tag{42 - b}$$

The time derivative of the siding manifold can be obtained as follows:

$$S' = a_1\frac{E}{L} + (1-u)\left[-a_1\frac{v_O}{L} + \frac{a_2 i_L}{C} - \frac{a_4}{LC}(1-u)i_L\right] - \frac{a_2 v_O}{RC} + a_3(v_O - V_d) + \frac{a_4 v_O}{L}u' + \frac{a_4(1-u)v_O}{RLC} \tag{43}$$

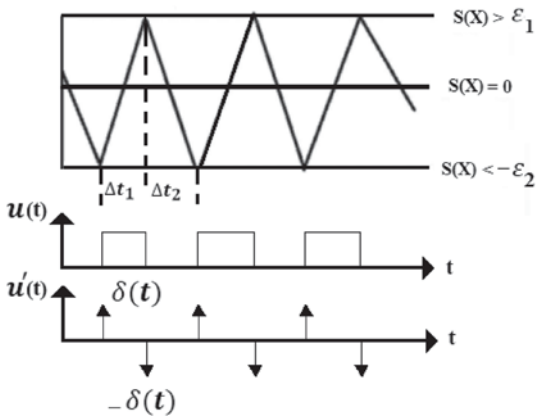

Figure 5. The sliding mode operation in CCM.

When S becomes positive, then $u = 1$ and $u' = \delta(t)$. Also, when S becomes negative, then $u = 0$ and $u' = -\delta(t)$, where $\delta(t)$ is the impulse function. The equations for $S'|_{u=0}$ and $S'|_{u=1}$ can be given as follows:

$$S'|_{u=1} = a_1\frac{E}{L} - \frac{a_2 v_O}{RC} + a_3(v_O - V_d) + \frac{a_4 v_O}{L}\delta(t) \tag{44 - a}$$

$$S'|_{u=0} = a_1\frac{E}{L} + \left[-a_1\frac{v_O}{L} + \frac{a_2 i_L}{C} - \frac{a_4}{LC}i_L\right] - \frac{a_2 v_O}{RC} + a_3(v_O - V_d) - \frac{a_4 v_O}{L}\delta(t) + \frac{a_4 v_O}{RLC} \tag{44 - b}$$

From (44) it is observed that the speed of the sliding manifold is dependent to the impulse function. Hence, the sliding mode operation happens with a very high speed around origin. Hence, the theoretical frequency of the SMC converges to infinite despite of having large time delays in electrical circuits or equivalently, adopting large hysteresis bandwidths. In practice, time delays of practical circuits increase the actual hysteresis bandwidths. The mean of (44) is obtained as follows:

$$\langle S'\rangle|_{u=1} = a_1\frac{E}{L} - \frac{a_2 V_d}{RC} + \frac{a_4 V_d}{L}\frac{f_s}{U} \tag{45 - a}$$

$$\langle S'\rangle|_{u=0} = a_1\frac{E}{L} + \left[-a_1\frac{V_d}{L} + \frac{a_2 I_L}{C} - \frac{a_4}{LC}I_L\right] - \frac{a_2 V_d}{RC_2} - \frac{a_4 V_d}{L}\frac{f_s}{1-U} + \frac{a_4 V_d}{RLC} \tag{45 - b}$$

By using (41), the frequency equation can be determined as:

$$f_s = \frac{1}{\frac{\varepsilon_1+\varepsilon_2}{a_1\frac{E}{L}-\frac{a_2V_d}{RC}+\frac{a_4V_df_s}{LU}} - \frac{\varepsilon_1+\varepsilon_2}{a_1\frac{E}{L}-\frac{V_d}{L}\left(a_1+a_4\frac{f_s}{1-U}\right)+\left(\frac{a_2}{C}-\frac{a_4}{LC}\right)\frac{V_d^2}{RE}-\frac{a_2V_d}{RC}+\frac{a_4V_d}{RLC}}} \quad (46)$$

By using numerical techniques, (46) can be solved. The parameters of the converter are given in Table 1. Figure 6 depicts the frequency of the proposed IHFSMCC versus the mean of hysteresis bandwidths of bang-bang modulator. From this figure, it is clear that the parameter a_4 has a large effect on the frequency. The frequency of the traditional SMC can be increased only around the zero bandwidth by reducing time delays of control circuits. However, in practical applications, there exists an inherently large time delay in circuits, introducing non-ideal components.

4. Simulations

In this section, we discuss the effectiveness of the developed IHFSMCC for the Boost converter through the simulation results. The proposed system including the hysteresis modulation is implemented using the PSIM-program. Also, a simple SMC [26–28] is used for comparison. The nominal parameters of the DC/DC boost converter are presented in tables 1 and 2. The parameters of the IHFSMCC are chosen as: $a_1 = 1, a_2 = 0.2, a_3 = 40, a_4 = 0.2L, \varepsilon_1 = \varepsilon_2 = 2.6$. The simple SMC is designed for comparison. Also, the sampling frequency is selected as 40 kHz for the simple control scheme. The selection criterion of the parameters of the controllers is to guarantee disturbance rejection, robustness and a satisfactory balance among tracking performance.

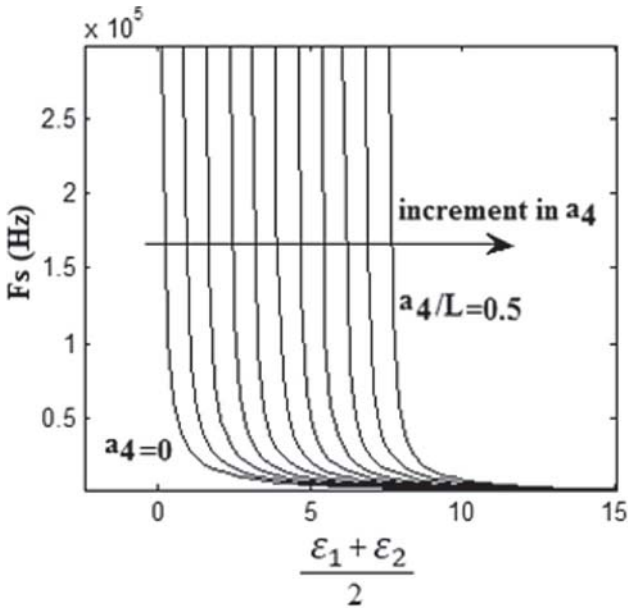

Figure 6. The converter frequency with the proposed IHFSMCC for $V_d = 30$ V, $R = 48\ \Omega$, $E = 9$ V and different values of a_4.

Figures 7a-c represent the response curves of the converter voltage with the developed IHFSMCC and simple SMC for $V_d = 25$, 30 and $35V$, respectively. As shown in figure 7a, the load voltage with the simple control scheme cannot track the reference voltage and there exists a steady error of about 2 V. Furthermore, figure 7b depicts that the voltage response with the simple controller has a large steady error of 1.5 V for $V_d = 30$V. Also, in figure 7c, the steady state error of the converter voltage with the simple controller increases to 6 V for $V_d = 35$V. However, for all the simulations, the output voltage of the Boost converter with the IHFSMCC tracks accurately its reference signal with settling time of 6, 10 and 20 ms for $V_d = 25$, 30 and 35 V, respectively. It is remarked that the voltage tracking performance is effected by parametric resistances of power components and sampling frequency of the controller. Hence, the simple SMC cannot well regulate the output voltage of the converter against large uncertainties. An effective way to eliminate the effects is the utilization of an improved SMC with fast sampling time.

Figures 8a-c are presented to show the steady state waveform of the inductor current of the converter with both the controllers for $V_O = 25$, 30 and 35 V, respectively. It is understood from the figures that the inductor current ripple of the converter under the simple controller is very large for all the conditions and the simple SMC with the limited sampling frequency cannot keep the converter at continuous current conditions. It is a bad property of the digital implementation strategy presented in [26–28]. However, using proposed strategy, the converter can work in continuous current mode. Also, figures 9a and b show the enlarged steady state waveform of the inductor current and output voltage of the converter using the IHFSMCC and simple SMC, respectively. It can be seen that the switching frequency of the converter is 300KHz for improved method closer to theoretical selected value shown in table 1 and 12.5 kHz for simple method closer to the results presented in [27]. These figures show that the low switching frequency results in a higher ripple in the current and voltage,

Table 2. The parasitic elements of the Boost converter for simulations

Symbol	name	Value
R_L	The equivalent series resistance of inductor	0.2 Ω
R_C	The equivalent series resistance of capacitor	0.06 Ω
R_S	The equivalent series resistance of switch	0.1 Ω
R_D	The equivalent series resistance of diode	0.1 Ω
V_D	The forward voltage of diode	0.5 V

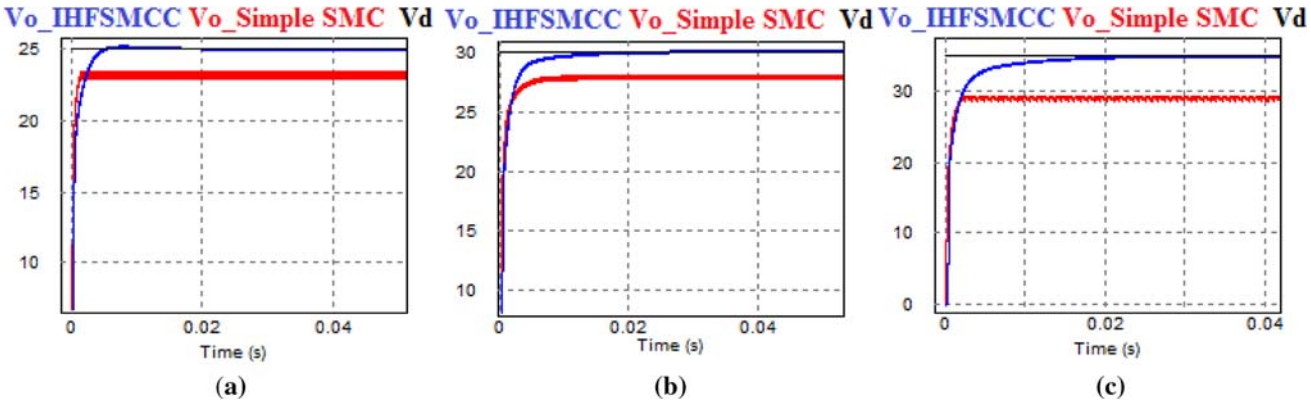

Figure 7. The simulated response of the input curent and output voltage of the Boost converter with the proposed IHFSMCC and simple SMC for $R = 48\ \Omega$, $E = 9$ V; (a) $V_d = 25$ V; (b) $V_d = 30$ V; (c) $V_d = 35$ V.

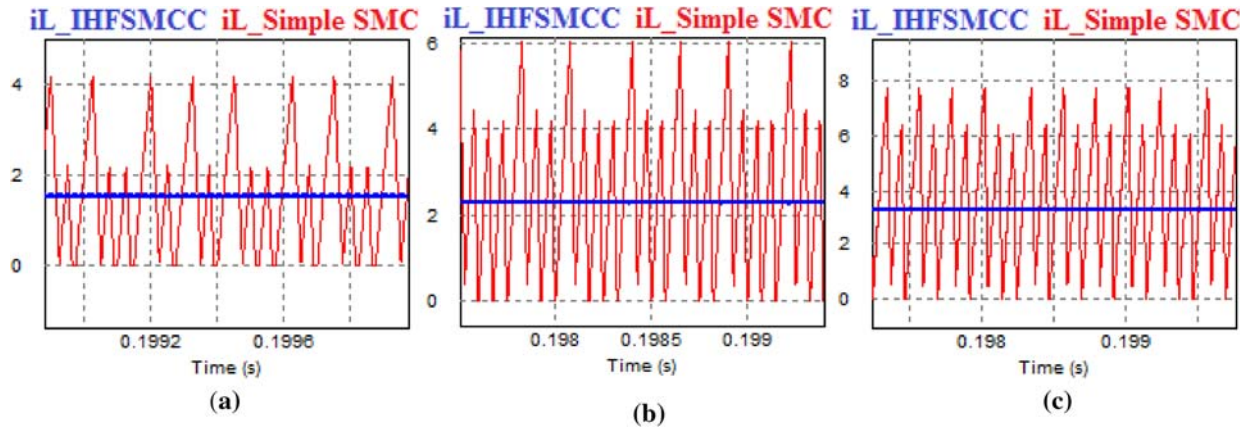

Figure 8. The instanteos waveform of the input curent of the Boost converter under the proposed IHFSMCC and simple SMC for $R = 48\ \Omega$, $E = 9$ V; (a) $V_O = 25$ V; (b) $V_O = 30$ V; (c) $V_O = 35$ V.

distortion of the voltage and inductor core saturation problem in practice.

5. Experimental results

In this section, the experiential results for the proposed system are provided for discussion. A laboratory model has been implemented to confirm the simulation results. The experimental model set-up is constructed with the same system parameters presented in the previous section. The validation of the suggested method is done for start-up transient condition and steady state region performance. Figure 10 shows the laboratory set-up of the proposed system. The circuit components of the proposed system are as follows:

Current sensor: ACS712-20A; S: IRFZ44N; D1, D2, D3: 1N5822; C1, C2: 100 μF/10V (electrolytic and plain polyester type); L1: 330 μH/5 A (ferrite core); Op Amp: LF351; Hysteresis Modulator: LM399; Gate Driver: TLP250

The analogue construction of the developed system for the Boost converter is shown in figure 10. The system operation is described as: the output voltage, inductor voltage and input inductor current of the Boost converter are sensed by using potentiometer and current sensor. The output voltage is subtracted from the reference voltage using LF351. Next, the voltage error e_2 is produced and it is passed to a PI controller. Also, the positive and negative polarities of the inductor voltage are directly sensed and subtracted from each other using two Op-Amps to produce the inductor voltage. Furthermore, input inductor current i_L is sensed using a current sensor and the output of the current sensor is adjusted using an Op-Amp. Then, the output voltage error, input current and inductor voltage are added together to construct the sliding manifold using an OP-Amp. The derived sliding manifold is compared using LM339 IC to produce the control input for the converter switch. The hysteresis comparator is implemented using the

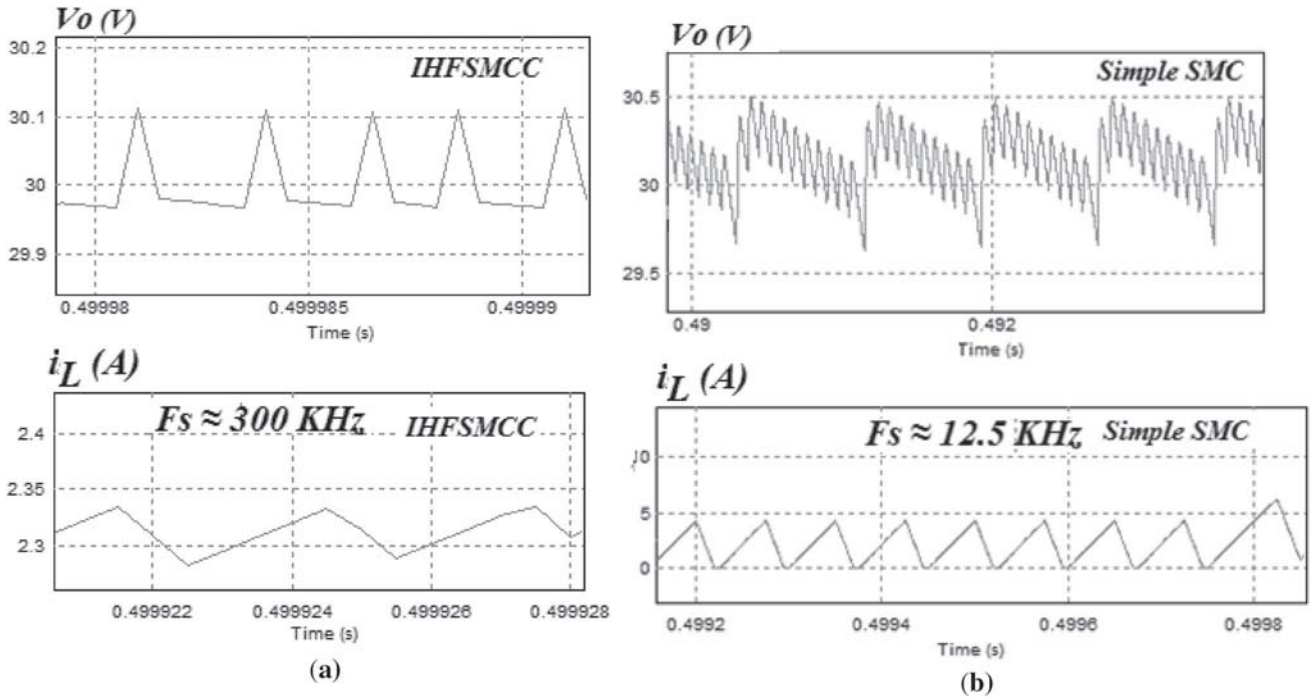

Figure 9. The magnified waveform of the curent and voltage of the Boost converter for $R = 48\ \Omega$, $E = 9V$, $V_O = 30V$; (a) $V_O = 35V$; (a) with the proposed IHFSMCC; (b) with the simple SMC.

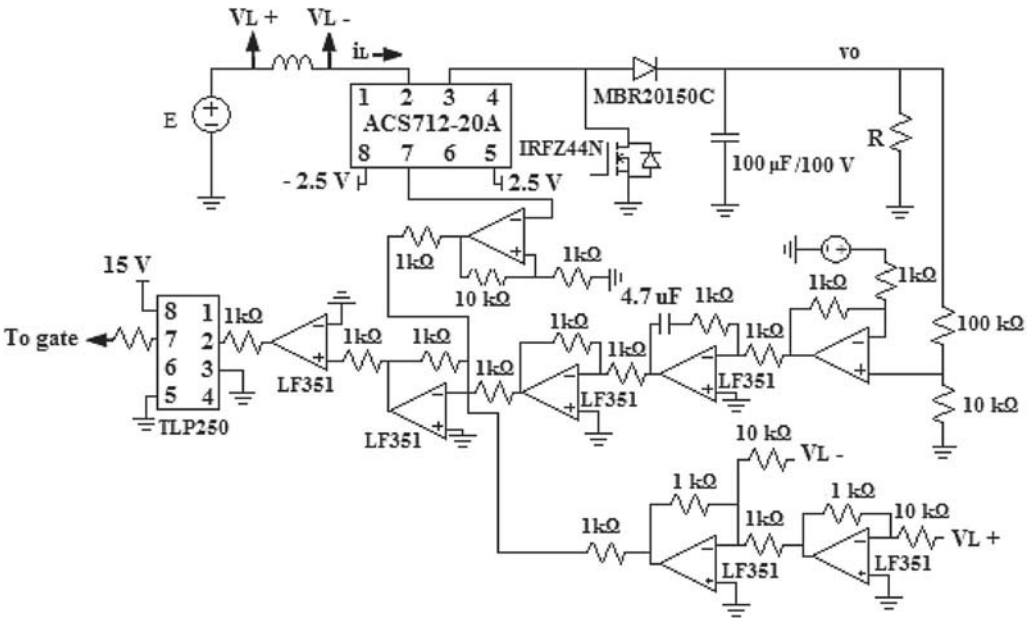

Figure 10. Basic structure of the Boost converter under the IHFSMCC in analogue platform.

LM399 that $\delta = R_1 V_{CC}/(R_1 + R_2)$ (used to set the nominal switching frequency for the converter). The generated signal is connected to the switch by the optocoupler (TLP250) and gate resistance.

Using the IHFSMCC, the switching frequency is changed to control the converter current and regulate the load voltage. Figures 11a-c illustrate the practical response of the current and voltage of the Boost converter under the designed IHFSCC during transient region. All tests are performed for $R = 48\ \Omega$. Consider the initial condition of the converter as: $v_O(0) \approx 9$ V and $i_L(0) \approx 0$. The input voltage is set at 9 V. The converter response for steady

operation point of $v_O = 25$ V is shown in figure 11a. From this figure, it is clear that the current and voltage have no overshoot. Moreover, the voltage of the Boost converter has a small settling time of nearly 50 ms. Also, the experimental behavior of the current and voltage of the converter is shown in figure 11b for steady operating condition of $v_O = 20$ V. It can be seen from this figure that the voltage has a time delay of nearly 40 ms with no overshoot. The initial condition of the converter is adjusted at $v_O(0) \approx 15$ V and $i_L(0) \approx 0$. Consider $E = 15$ V. The start-up behavior of the converter with the designed IFHSMCC is depicted in figure 11c. It is evident that the system response has a settling time of 50 ms with excellent dynamical behavior. The aforementioned tests confirm that as predicted theoretically, the improved SMC can enhance the voltage of the Boost converter by eliminating the steady state error pf the voltage with fast response and satisfactory behavior, despite of the parasitic effects.

Figures 12a-c show the response of the converter voltage for input voltage step changes. Figure 12a depicts the practical response of the voltage for V_O=35 V, R=96Ω and source voltage variation from 11 to 18 V. For this result, the voltage has an overshoot of nearly 3 V and settling time of 25 ms. Figure 12 b illustrates the experimental behavior of the voltage for V_O = 35 V, R = 36 Ω and input voltage variation from 10 to 18 V. From this figure, it can be inferred that the voltage has an overshoot of about 5 V with settling time of nearly 50 ms. The dynamical behavior of the voltage for V_O=35 V, R=96 Ω and input voltage variation from 12 to 7.5 V is illustrated in figure 12c. This result shows that the voltage has an overshoot of nearly 3V and time delay of nearly 40 ms.

Figure 13a shows the voltage response for E=12 V and R=96 Ω and voltage change from nearly 27 to 55 V and vice versa during transient region. Here, the voltage overshoot is less than 2 V with rise time of nearly 10 ms. Figure 13b shows the practical response of the voltage for E=12 V and R=96 Ω and the voltage variation from nearly 20 to 40 V. For this experiment, the voltage overshoot and settling time are nearly 6 V and 20 ms. In figure 13c, the voltage behavior is shown for E=12 V, R=36Ω and the voltage change from 20 to 40 V. For this test, the settling time is nearly 40 ms with no overshoot.

The performance of the Boost converter under the proposed IHFSMCC and conventional SMC in steady region is shown in figures 14 and 15. It is again noticed that the conventional sliding mode methods cannot control low power DC/DC converters at high frequencies. Consider the Boost converter with operating point of $V_O = 25$ V, $R = 48\ \Omega$ and $E = 9$ V. Figures 14a and b depict the steady response of the input current, output voltage, switching signal and sliding manifold of the Boost converter with designed IHFSMCC and conventional method, respectively. Here, it is understood that the frequency of the hysteresis modulator of the common SMC is about 5.2 kHz with maximum bandwidth of nearly 1 V. However, the frequency of the IHFSMCC is about 270 kHz with maximum bandwidth of about 2 V. Also, the steady state behavior of the converter under both the controllers is shown in figure 15 for $R = 48\ \Omega$, $V_O = 20$ V and $E = 9$ V. Figure 15a illustrates that that the converter frequency using the simple approach is about 5.2 KHz. However, figure 15b shows that the converter frequency with the improved method is nearly 250 KHz. Also, form Figures 14 and 15, it is seen that the practical hysteresis bandwidth of the IHFSMCC is larger than the practical hysteresis bandwidth of the simple SMC.

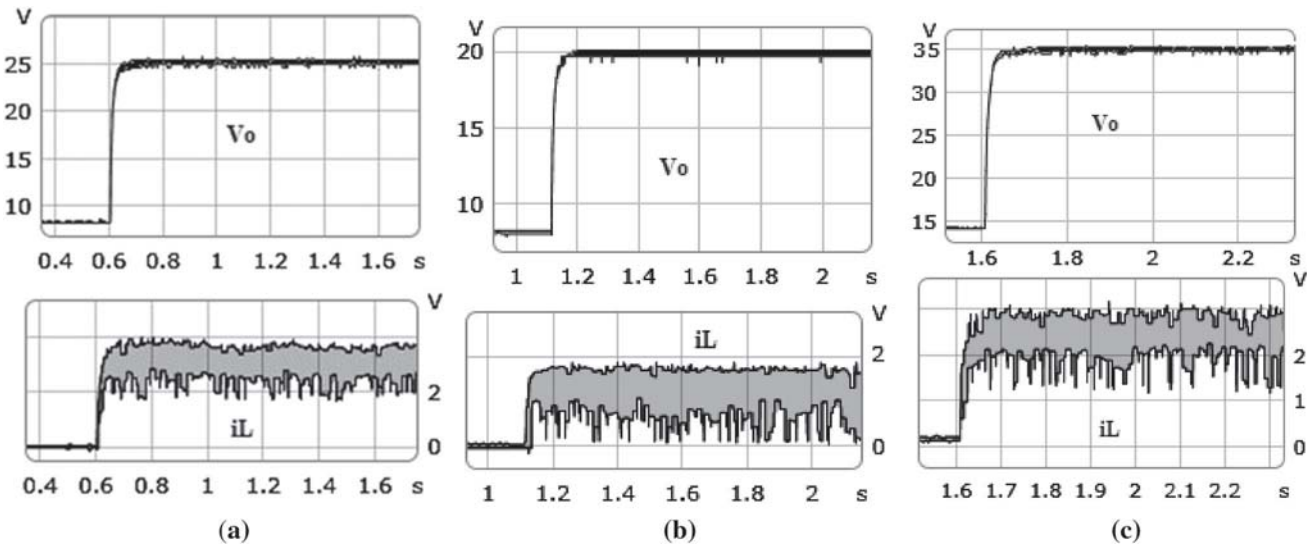

Figure 11. The transient response of the inductor current and output voltage of the converter with the IHFSMCC for $R = 48\ \Omega$; (a) $E = 9$ V and $V_O = 25$ V; (b) $E = 9$ V and $V_O = 20$ V; (c) $E = 15$ V and $V_O = 35$ V; (d) $E = 18$ V and $V_O = 35$ V

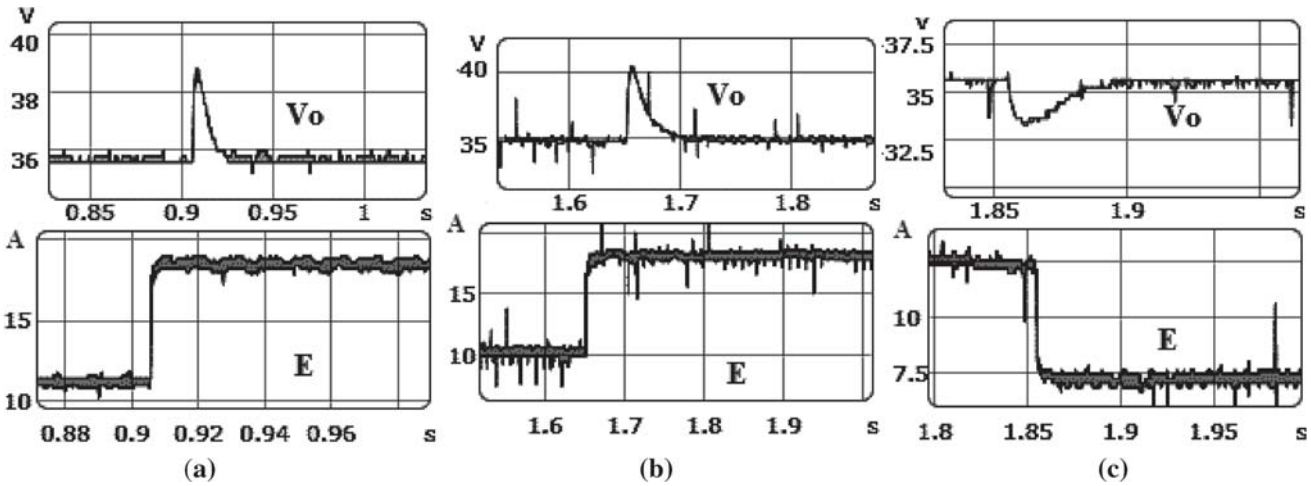

Figure 12. Responses of the output voltage for V_O=35 V and input voltage variations; (a) R=96 Ω, E=11 to 18 V; (b) R=36 Ω, E=10 to 18 V; (c) R=96 Ω, E=12 to 7.5 V.

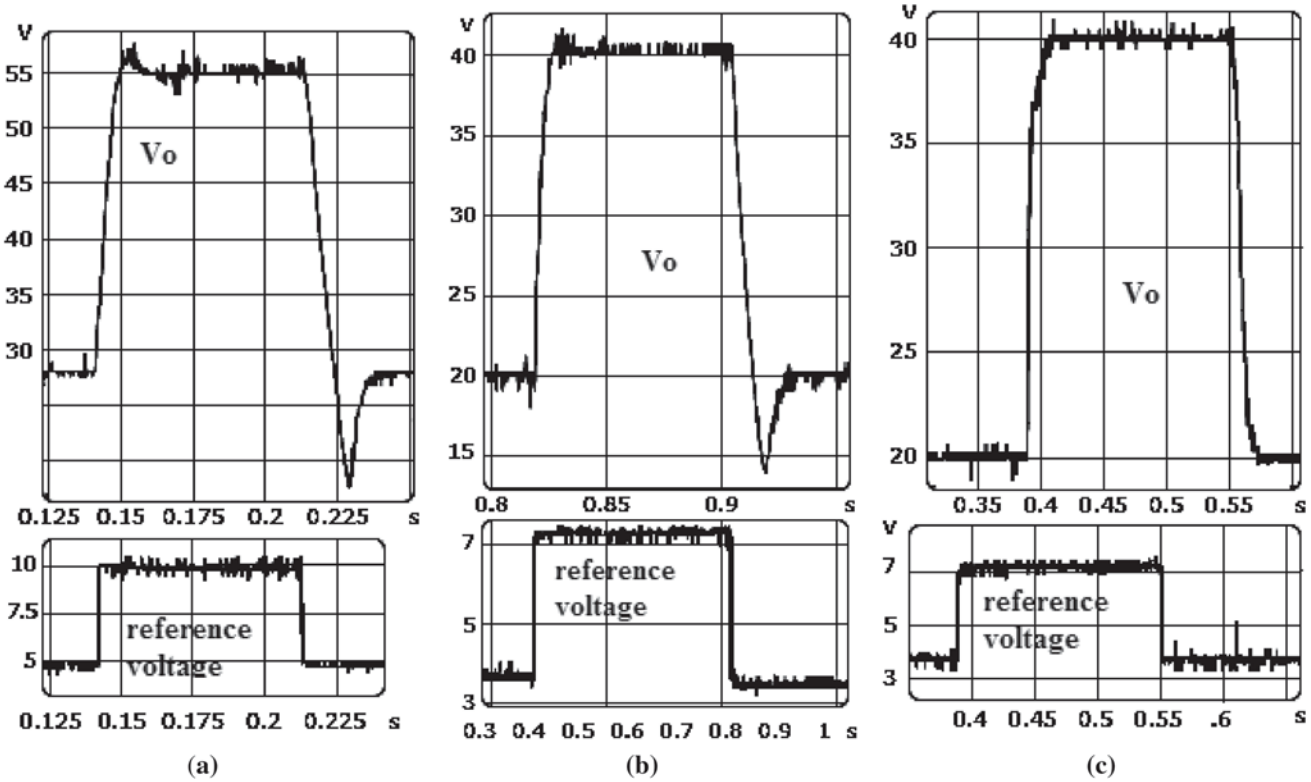

Figure 13. Voltage response against the voltage reference change; (a) E=12 V, R=96 Ω and V_O = 27 V to 55 V; (b) E=12 V, R = 96 Ω and V_O = 40 to 20 V; (c) E = 12 V, R = 36 Ω and V_O = 20 V to 40 V.

6. Discussions

This section discusses the advantages and drawback of the suggested standard IHFSMCC for the Boost converter as compared with conventional SMCs. The important merits of the IHFSMCC is its high robustness and the simplicity of the controller design. Unlike traditional voltage mode and current mode controllers which need complicated procedures to estimate the coefficients of the controller parameter, the suitable parameters of the proposed controller can be exactly determined from the dynamic equations. Also, since the IHFSMCC is designed based on the large-signal model of the Boost converter, it will be stable in transient region and highly robust against large uncertainties and variations of the working point of the converter. This is a key merit over traditional voltage mode

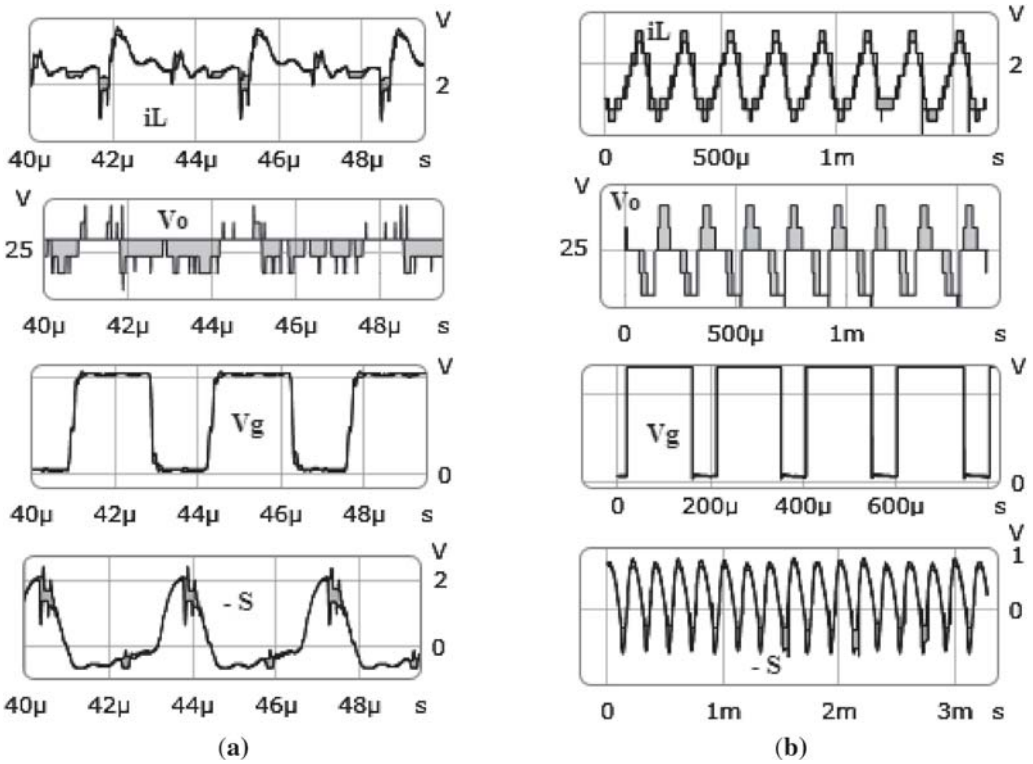

Figure 14. Voltage response in steady region for $R = 48\ \Omega$, $V_O = 25$ V and $E = 9$ V; (a) The conventional SMC; (b) The proposed IHFSMCC.

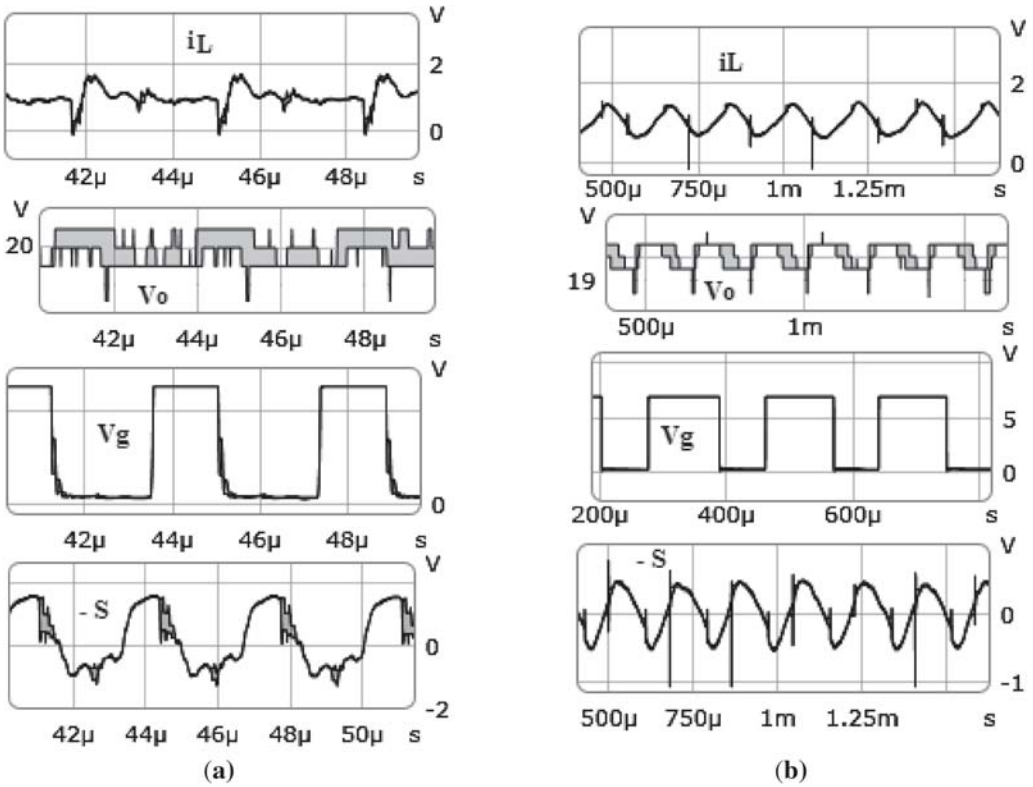

Figure 15. Voltage response in steady region for $R = 48\ \Omega$, $V_O = 20$ V and $E = 9$ V; (a) The conventional SMC; (b) The proposed IHFSMCC.

and current mode approaches which usually fail to achieve satisfactory response under parameter uncertainties or output voltage variations because they are developed based on the small signal models of the converter. Other advantage of the proposed IHFSCC is that it gives the feasibility for the achievement of a zero steady state voltage error. It is due to the application of the proper sliding manifold in the design. The other good feature of the proposed IHFSMCC is that it guarantees the continuous current mode operation of the Boost converter, particularly at light loads. Additionally, it considerably reduces the requirements of EMI filters, because of its wide bandwidth spectrum effects. This idea arises due to the fact that the proposed hysteresis modulation method leading to high switching frequency.

A main drawback of the proposed controller is that the steady state switching frequency is influenced by the converter parameters and its operating point. The non-constant switching frequency makes the design of the input and output filters of the converter more complicated. The variable switching frequency problem can be solved by adopting the parabolic SMC methods. The parabolic technique could be used based on the proposed sliding manifold of this paper in future works by researchers.

7. Conclusion

This paper presents a unified method to design an improved hysteresis modulation-based sliding mode current controller for the voltage regulation of a Boost converter in continuous conduction mode at high frequencies despite having large practical hysteresis bandwidth based on the analogue construction. The main contribution of this study is that a straightforward formulation based on sliding mode concepts is described for a complicated nonlinear system of third-order which can be used to predict the system stability. However, it can be applied to similar high order systems. Using an integral term in the sliding manifold of the controller, the performance of the SMC is improved to regulate the output voltage of the converter without any steady error. In practice, there are time delays introduced by electrical devices. These propagation delays increase the practical hysteresis bandwidth of a SMC and restrict maximum switching frequency of the controller and as a result, current and voltage ripples of the converter increase. In order to solve these problems, a feedback control scheme according to the inductor voltage is added to the sliding manifold. The appropriate coefficients of the proposed SMC for generating an under damped system have been obtained by using the Filippov's criterion. Hence, the transient response of the output voltage caused by circuit component variations is predictable. Also, a comparison between digital and analogue control schemes is provided. It is shown that a low-cost analogue implementation have many advantages such as: more accuracy and high sampling frequency which reduce voltage error and current ripple. Simulation and experimental results show high accuracy of the controller for a fast behavior, excellent transient response and strong system robustness.

References

[1] Dawande M, Donescu V, Yao Z and Rajagopalan V 1997 Recent advances in simulation of power electronics converter systems. *Sadhana - Acad. Proc. Eng. Sci.* 22: 689–704

[2] Veerachary M 2011 Fourth order buck converter for maximum power point tracking applications. *IEEE Trans. Aerosp. Electron. Syst*. 47: 896–911

[3] Yang J and Do H 2013 Analysis and design of a high-efficiency zero-voltage-switching step-up DC/DC converter. *Sadhana- Acad. Proc. Eng. Sci.* 38: 653–665

[4] Min R, Tong Q, Zhang Q, Chen C, Zou X and Lv D 2018 Corrective frequency compensation for parasitics in boost power converter with sensorless current mode control. *Int. J. Electr. Power Energy Syst*. 96: 274–281

[5] Goudarzina A, Nasiri H and Abjadi N 2016 Design and implementation of a constant frequency sliding mode controller for a Luo converter. *Int. J. Eng*. 29: 202–210

[6] Forouzesh M, Siwakoti Y, Gorji S A, Blaabjerg F and Lehman B 2017 Step-up DC/DC converters: a comprehensive review of voltage boosting techniques, topologies, and applications. *IEEE Trans. Power Electron*. 32: 9143–9178

[7] Lee C, Yang J and Jiang J 2010 Assessment of PEM fuel cells-based DC/DC power conversion for applications in AUVs. *IEEE Trans. Aerosp. Electron. Syst*. 46: 1834–1847

[8] Wang J M, Chien H C, Wu S T, Yen S C and Lin J Y 2016 Analysis and design of a boost PFC converter with sample-and-hold control techniques. *Int. Trans. Electr. Energy Syst*. 25: 3122–3138

[9] Ramasamy M and Thangavel S 2012 Photovoltaic based dynamic voltage restorer with power saver capability using PI controller. *Int. J. Electr. Power Energy Syst*. 36: 51–59

[10] Xia C, Geng Q, Gu X, Shi T and Song Z 2012 Input output feedback linearization and speed control of a surface permanent magnet synchronous wind generator with the boost chopper converter. *IEEE Trans. Ind. Electron*. 59: 3489–3500

[11] Yi L, Zhao J and Ma D 2007 Adaptive backstepping sliding mode nonlinear control for buck DC/DC switch power converter. *IEEE Int. Conf. Control. Auto*. pp. 1198-1201

[12] Fadil H, Giri F, Magueri O and Chaoui F 2009 Control of DC/DC power converters in the presence of coil magnetic saturation. *Control Eng. Practice*. 17: 849-862

[13] Hallworth M and Shirsavar S 2012 Microcontroller-based peak current mode control using digital slope compensation. *IEEE Trans. Power Electron*. 20: 3340–3351

[14] Chen S 2012 Small-signal model for a flyback converter with peak current mode control. *IET Power Electron*. 7: 805–810

[15] Li Y, Vannorsdel K, Zirger A, Norris M and Maksimovic D 2012 Current mode control for boost converters with constant power loads. *IEEE Trans. Circuits Syst. I-Regul. Pap*. 59: 198–206

[16] Mandal K, Banerjee S and Chakraborty C 2014 A new algorithm for small-signal analysis of DC/DC converters. *IEEE Trans. Ind. Inform*. 10: 628–636

[17] Wu L, Mazumder S K and Kaynak O 2017 Sliding mode control and observation for complex industrial systems part 1. *IEEE Trans. Ind. Electron*. 64: 229–237

[18] Tan S, Lai Y M, Tse C K, Martinez-Salamero L and Wu C 2007 A fast response sliding mode controller for Boost Type converters with a wide range of operating conditions. *IEEE Trans. Power Electron*. 54: 3276–3286

[19] Tan S, Lai Y M and Tse C K 2008 Indirect sliding mode control of power converters via double integral sliding surface. *IEEE Trans. Power Electron*. 23: 600–611

[20] Mohanty P and Panda A 2016 Fixed frequency sliding mode (SM) control scheme based on current control manifold for improved dynamic performance of boost PFC converter. *IEEE J. Emerg. Sel. Top. Power Electron*. 5: 576–586

[21] Nasiri H, Goudarzian A, Pourbagher R and Derakhshandeh S Y 2017 PI and PWM sliding mode control of POESLL converter. *IEEE Trans. Aerosp. Electron. Syst*. 53: 2167–2177

[22] Liu J, Yin Y, Luo W, Vazquez S, Franquelo L G and Wu L 2017 Sliding mode control of a three phase ac/dc voltage source converter under unknown load conditions: industry applications. *IEEE Trans. Syst. Man Cybern. Syst*. 48: 1771–1780

[23] Chen Z 2012 PI and sliding mode control of a Cuk converter. *IEEE Trans. Power Electron*. 27: 3695–3703

[24] Wang G and Li Y W 2010 Parabolic PWM for current control of voltage-source converters (VSCs). *IEEE Trans. Ind. Electron*. 57(100): 3491–3496

[25] Zhang L, Gu B, Dominic J, Chen B, Zheng C and Lai J S 2014 A dead-time compensation method for parabolic current control with improved current tracking precision. *IEEE Trans. Power Electron*. 30: 195–202

[26] Bhat S and Nagaraja H N 2015 DSP based proportional integral sliding mode controller for photo-voltaic system. *Int. J. Electr. Power Energy Syst*. 71: 123–130

[27] Banerjee B, Kotecha R M and Weaver W W 2016 Digital memory look-up based implementation of sliding mode control for DC/DC converters. *Control Eng. Practice*. 54: 1–11

[28] Prakash L, Sundaram A M and Jesudaiyan S 2017 A simplified time-domain design and implementation of cascaded PI-sliding mode controller for DC/DC converters used in off-grid photovoltaic applications with field test results. *Sadhana - Acad. Proc. Eng. Sci.* 42: 687–699

[29] Mohan N, Undeland T M and Robbins W P 1995 *Power electronics: converters, applications and design*. Wiley, New York

[30] Knalil K 2002 *Nonlinear Systems*. Upper Saddle River, NJ: Prentice-Hall